

Robust speed estimation of an induction motor under the conditions of rotor time constant variability due to the rotor deep-bar effect

JAROSŁAW ROLEK¹, GRZEGORZ UTRATA², ANDRZEJ KAPLON¹

¹*Department of Industrial Electrical Engineering and Automatic Control
Kielce University of Technology
7 Tysiąclecia Państwa Polskiego Ave., 25-314 Kielce, Poland*

²*Faculty of Electrical Engineering, Czestochowa University of Technology
17 Armii Krajowej Ave., 42-200 Czestochowa, Poland
e-mail: jrolek@tu.kielce.pl, grzegorz.ustrata@pcz.pl, akaplon@tu.kielce.pl*

(Received: 15.05.2019, revised: 04.11.2019)

Abstract: Accurate information on Induction Motor (IM) speed is essential for robust operation of vector controlled IM drives. Simultaneous estimation of speed provides redundancy in motor drives and enables their operation in case of a speed sensor failure. Furthermore, speed estimation can replace its direct measurement for low-cost IM drives or drives operated in difficult environmental conditions. During torque transients when slip frequency is not controlled within the set range of values, the rotor electromagnetic time constant varies due to the rotor deep-bar effect. The model-based schemes for IM speed estimation are inherently more or less sensitive to variability of IM electromagnetic parameters. This paper presents the study on robustness improvement of the Model Reference Adaptive System (MRAS) based speed estimator to variability of IM electromagnetic parameters resulting from the rotor deep-bar effect. The proposed modification of the MRAS-based speed estimator builds on the use of the rotor flux voltage-current model as the adjustable model. The verification of the analyzed configurations of the MRAS-based speed estimator was performed in the slip frequency range corresponding to the IM load adjustment range up to 1.30 of the stator rated current. This was done for a rigorous and reliable assessment of estimators' robustness to rotor electromagnetic parameter variability resulting from the rotor deep-bar effect. The theoretical reasoning is supported by the results of experimental tests which confirm the improved operation accuracy and reliability of the proposed speed estimator configuration under the considered working conditions in comparison to the classical MRAS-based speed estimator.

Key words: deep-bar effect, estimation, induction motors, motor drives



1. Introduction

The development of the field-oriented control strategies of Induction Motors (IMs) have contributed to their widespread employment in modern drive applications. In such applications, IM speed is not only the motor drive feedback signal but it is also required for proper operation of IM field-oriented control. IM speed is generally obtained with the use of measuring sensors. Consequently, the correct operation and reliability of the motor drive closely depend on failure-free operation of the speed sensor. IM speed estimation schemes can be employed in vector controlled IM drives in order to provide drive operation in case of speed sensor failure. Such schemes also enable eliminating the direct speed measurement, for instance, in low cost motor drives or drives operating in difficult environmental conditions.

Various schemes for IM speed estimation were proposed in the literature [1]. The IM speed estimation schemes can be classified in two groups. The first group is represented by the schemes based on the frequency analysis of rotor slot harmonics contained in stator currents or induced voltages [2–4] or airgap eccentricity components included in inverter supply currents [5]. In such an approach, the accuracy of speed estimation is not dependent on variability of IM electromagnetic parameters and this is the primary advantage of the schemes assigned to the first group. However, these schemes use complex signal processing procedures. What is more, the adequate adaptation of stator windings is required for some of them [4]. This fact further complicates their application in a motor drive control structure.

The second group includes estimation schemes which are formulated on the basis of IM mathematical models. In this case, the IM speed is usually estimated simultaneously with the rotor flux space vector by means of the Model Reference Adaptive System (MRAS) based estimator [6–15], an extended observer [16–18] or an extended Kalman filter [19, 20].

In the group of the model-based schemes for IM speed estimation, the classical MRAS-based speed estimator [6] is characterized by an uncomplex algorithm, and thus its application in a motor drive control structure does not pose too many difficulties. On the other hand, the estimator of this type is sensitive to IM electromagnetic parameter variability [7, 8]. The theoretical considerations provided in these works also indicated the tendency of the classical MRAS-based speed estimator [7] or the motor drive where such an estimator is employed [8] to lose stability in the case of erroneous representation of IM electromagnetic parameters by equivalent parameters of the estimator mathematical model.

The issue of robustness enhancement of the MRAS-based speed estimator to IM electromagnetic parameter variability constituted the trigger to extensive investigations for many research centres worldwide. In consequence, various modifications of the MRAS-based speed estimator were developed [7–14]. Some schemes were extended by algorithms enabling tracking variability of IM electromagnetic parameters as in [15].

The paper presents the selected results of the work which aimed to improve the robustness of the MRAS-based speed estimator to rotor electromagnetic parameter variability resulting from the rotor deep-bar effect. In case of field-oriented controlled IMs, such variability occurs during torque transients when slip frequency is not controlled within the set range of values. This problem concerns especially squirrel-cage IMs which rotor bars are large enough to incorporate high rotor current.

In this paper, the modified MRAS-based speed estimator is proposed and investigated. The modification builds on the use of the so called Full Order Open-Loop Flux Observer [21] as the adjustable model and is encouraged by the theoretical reasoning including frequency-domain analysis. The accuracy and reliability of the proposed configuration of the MRAS-based estimator are verified through experimental tests. The classical MRAS-based speed estimator [6] is employed as the baseline in the presented comparative studies.

2. Mathematical models of the MRAS-based speed estimator

2.1. Classical MRAS-based speed estimator

The classical MRAS-based speed estimator employs two independent models of the rotor flux space vectors: the voltage (1) and current (2) models [6]. If expressed in the orthogonal coordinate system (α - β) stationary with respect to the stator $\omega_k = 0$ (indicated by the subscript “s”), these models take the following forms:

$$\underline{\Psi}_{2s}^{e(u)} = \frac{L_2}{L_\mu} \left(\int_0^t (\underline{U}_{1s} - R_1 \underline{I}_{1s}) dt - \sigma L_1 \underline{I}_{1s} \right), \quad (1)$$

$$\frac{d}{dt} \underline{\Psi}_{2s}^{e(i)} = \frac{R_2}{L_2} L_\mu \underline{I}_{1s} - \frac{R_2}{L_2} \underline{\Psi}_{2s}^{e(i)} + j\omega \underline{\Psi}_{2s}^{e(i)}, \quad (2)$$

$$\sigma = 1 - \frac{L_\mu^2}{L_1 L_2}, \quad (3)$$

where: \underline{U}_{1s} , \underline{I}_{1s} are the stator voltage and current space vectors, respectively, $\underline{\Psi}_{2s}$ is the rotor flux space vector, R_1 , R_2 stand for the stator and rotor resistances, respectively, $L_1 = L_{1\sigma} + L_\mu$, $L_2 = L_{2\sigma} + L_\mu$, L_1 , L_2 represent the stator and rotor self-inductances, respectively, $L_{1\sigma}$, $L_{2\sigma}$ are the stator and rotor leakage inductances, respectively, L_μ constitutes the magnetizing inductance, σ denotes the inductive leakage factor, ω_m is the IM speed (angular velocity), $j^2 = -1$, “j” represents the imaginary unit. The superscripts “ $e(u)$ ” and “ $e(i)$ ” denote rotor flux space vectors estimated by the voltage and current model, respectively.

In this paper, rotor physical quantities and electromagnetic parameters are referred to the stator.

Since the IM speed is not incorporated in the rotor flux voltage model (1), it serves as the reference model of the classical MRAS-based speed estimator. In contrast to the voltage model, the rotor flux current model (2) includes the IM speed and so it is applied as the estimator adjustable model. The outputs of the reference and adjustable models are then fed to the input of a properly formulated adaptation mechanism. The estimated speed ω_m^e , obtained from this adaptation mechanism, constitutes subsequently the input of the rotor flux current model (2). In this approach, the IM speed is adjusted based on errors between the rotor flux space vectors generated with the use of the reference and adjustable models of the MRAS-based speed estimator [6].

The adaptation mechanism of the MRA-based speed estimator, which general form is expressed by Equation (4), was developed in the work [6] on the basis of synthesis techniques for

MRAS structures grounded on the concept of hyperstability.

$$\omega_m^e = \Phi_2(\varepsilon_\alpha, \varepsilon_\beta) \int_0^t \Phi_1(\varepsilon_\alpha, \varepsilon_\beta) dt. \quad (4)$$

The demanded functions $\Phi_1(\varepsilon_\alpha, \varepsilon_\beta)$ and $\Phi_2(\varepsilon_\alpha, \varepsilon_\beta)$ of the adopted adaptation mechanism, ensuring the stable operation of the MRAS-based speed estimator with regard to the Popov's criterion, are as follows [6]:

$$\Phi_1(\varepsilon_\alpha, \varepsilon_\beta) = K_2(\varepsilon_\beta \Psi_{2\alpha}^{e(i)} - \varepsilon_\alpha \Psi_{2\beta}^{e(i)}), \quad (5)$$

$$\Phi_2(\varepsilon_\alpha, \varepsilon_\beta) = K_1(\varepsilon_\beta \Psi_{2\alpha}^{e(i)} - \varepsilon_\alpha \Psi_{2\beta}^{e(i)}), \quad (6)$$

$$\varepsilon_\alpha = \Psi_{2\alpha}^{e(u)} - \Psi_{2\alpha}^{e(i)}, \quad (7)$$

$$\varepsilon_\beta = \Psi_{2\beta}^{e(u)} - \Psi_{2\beta}^{e(i)}, \quad (8)$$

where: $\Psi_{2\alpha}, \Psi_{2\beta}$ stand for the components of the rotor flux space vector expressed in the coordinate system ($\alpha-\beta$) stationary with respect to the stator $\omega_k = 0$, $\varepsilon_\alpha, \varepsilon_\beta$ are the errors between the rotor flux space vector components determined by means of the reference and adjustable models of the MRAS-based speed estimator, K_1, K_2 denote the adaptation mechanism gain constants.

Consequently, the IM speed can be obtained with the use of the proportional plus integral controller which is fed by the appropriately formulated errors between the rotor flux space vector components, estimated with the use of the reference and adjustable models:

$$\omega_m^e = K_1(\Psi_{2\beta}^{e(u)}\Psi_{2\alpha}^{e(i)} - \Psi_{2\alpha}^{e(u)}\Psi_{2\beta}^{e(i)}) + K_2 \int_0^t (\Psi_{2\beta}^{e(u)}\Psi_{2\alpha}^{e(i)} - \Psi_{2\alpha}^{e(u)}\Psi_{2\beta}^{e(i)}) dt. \quad (9)$$

The schematic diagram of the classical MRAS-based speed estimator is presented in Fig. 1. This configuration will be referred to as the MRAS^(u-i) throughout this paper.

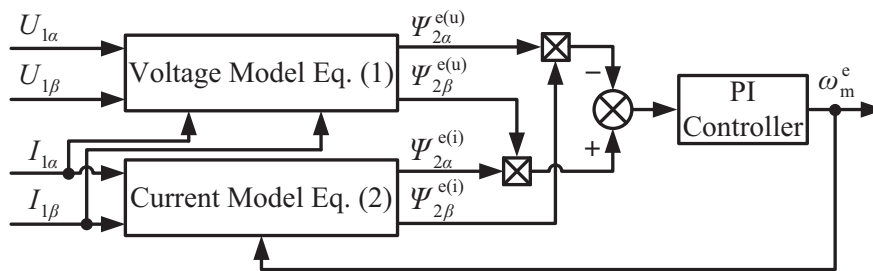


Fig. 1. The schematic diagram of the classical MRAS-based speed estimator

2.2. Modified MRAS-based speed estimator

The rotor flux current model (2) shows sensitivity to rotor resistance variability. This fact can be conveniently proved by means of the Frequency Response Function (FRF) of rotor flux

estimation as presented in the work [21]. This FRF is the ratio of the Laplace transforms of the rotor flux estimated by the model which electromagnetic parameters deviate from their actual values and the reference rotor flux which is estimated by the same model with actual electromagnetic parameters. Such an approach enables to evaluate the influence of variability of the IM individual electromagnetic parameters on accuracy of rotor flux estimation. With expressing the rotor flux estimation FRF as a function of slip frequency, sensitivity of the tested rotor flux models to rotor electromagnetic parameter variability can be assessed in the considered range of slip frequency. Since this paper is focused on the robustness verification of the tested configurations of the MRAS-based speed estimator to rotor electromagnetic parameter variability resulting from the rotor deep-bar effect, only the impact of rotor resistance R_2 and leakage inductance $L_{\sigma 2}$ deviations on rotor flux estimation accuracy was investigated in this study.

The rotor flux estimation FRF corresponding to the current model (2) takes the following form [21]:

$$\text{FRF}^{(i)} = \frac{\hat{\Psi}_{2s}^{e(i)}}{\underline{\Psi}_{2s}^{e(i)}} = \frac{\left(\frac{\hat{R}_2}{\hat{L}_2} L_\mu\right) \left(\frac{R_2}{L_2} + p - j\omega_m\right)}{\left(\frac{R_2}{L_2} L_\mu\right) \left(\frac{\hat{R}_2}{\hat{L}_2} + p - j\omega_m\right)}, \quad (10)$$

where: $\hat{L}_2 = \hat{L}_{2\sigma} + L_\mu$, p is the complex frequency and “ $\hat{}$ ” above individual symbols indicates the IM electromagnetic parameters which deviate from their actual values and also the rotor flux space vector which was estimated with the model where deviated electromagnetic parameters were applied.

For steady state operation, the complex frequency may be replaced by the stator frequency $j\omega_1$, and thus the rotor flux estimation FRF can be expressed as function of slip frequency ω_2 :

$$\text{FRF}^{(i)} = \frac{\hat{\Psi}_{2s}^{e(i)}}{\underline{\Psi}_{2s}^{e(i)}} = \left(1 + j \frac{L_2}{R_2} \omega_2\right) \left(1 + j \frac{\hat{L}_2}{\hat{R}_2} \omega_2\right)^{-1} \Big|_{p=j\omega_1}. \quad (11)$$

Figs. 2 and 3 presents the $\text{FRF}^{(i)}$ magnitude and phase characteristics received in the case of rotor resistance and leakage inductance deviations in the range of $\pm 50\%$ to $\pm 10\%$, respectively, from their actual values. In these figures, slip frequency is expressed in the per-unit (p.u.) system and the stator frequency was used as the based value. The presented FRF characteristic were determined with the use of the electromagnetic parameters of the tested squirrel-cage IM. These parameters are denoted as Set 1 and listed in Table 1. Near rated slip frequency, the rotor flux current model is sensitive to rotor resistance deviation from its actual values and introduces estimation errors of both the rotor flux magnitude and phase angle (Fig. 2). This fact takes on special significance during torque transients of field-oriented controlled IMs, when slip frequency exceeds its set range of values and rotor electromagnetic parameters vary due to the rotor-deep bar effect. This especially relates to large squirrel-cage IMs. On the other hand, the rotor flux current model is robust to rotor leakage inductance deviations for any operating conditions (Fig. 3).

The appropriate combination of the rotor flux voltage (1) and current (2) models leads to the rotor flux estimation scheme which was called the Full Order Open-Loop Flux Observer in the work [21]. When expressed in the orthogonal coordinate system ($\alpha-\beta$) stationary with respect to

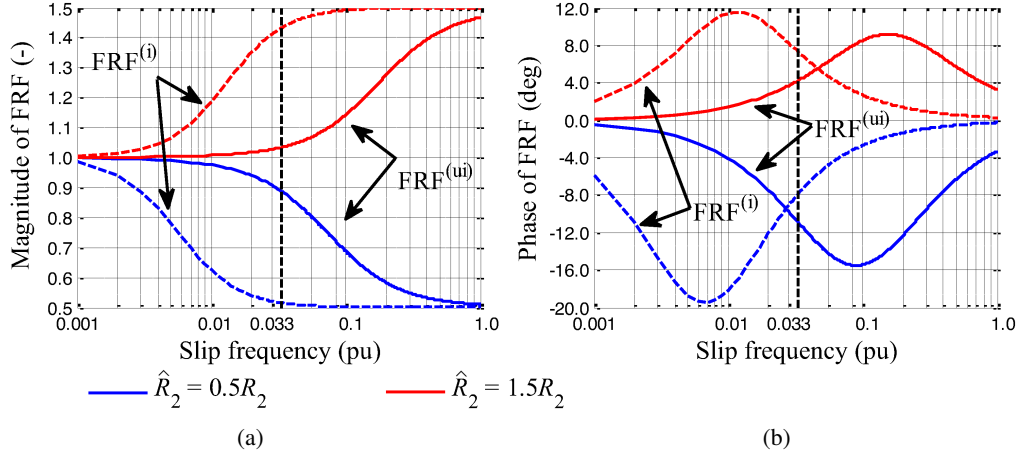


Fig. 2. The rotor flux estimation FRF characteristics corresponding to the rotor flux current and voltage-current models in the case of rotor resistance deviations from its actual value: (a) magnitude; (b) phase

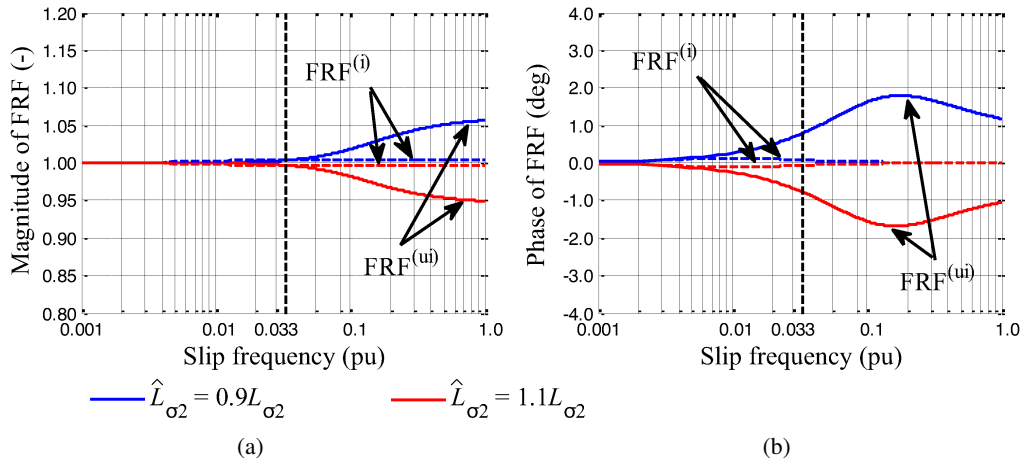


Fig. 3. The rotor flux estimation FRF characteristics corresponding to the rotor flux current and voltage-current models in the case of rotor leakage inductance deviations from its actual value: (a) magnitude; (b) phase

the stator $\omega_k = 0$, the resulting rotor flux voltage-current model is represented by the following system of equations:

$$\frac{d}{dt} I_{1s}^e = \frac{1}{\sigma L_1} \left[U_{1s} - \left(R_1 + \left(\frac{L_\mu}{L_2} \right)^2 R_2 \right) I_{1s}^e \right] + \frac{1}{\sigma L_1} \left[\frac{L_\mu}{L_2} \left(\frac{R_2}{L_2} - j\omega_m \right) \Psi_{2s}^{e(ui)} \right], \quad (12)$$

$$\frac{d}{dt} \Psi_{2s}^{e(ui)} = \frac{R_2}{L_2} L_\mu I_{1s}^e - \frac{R_2}{L_2} \Psi_{2s}^{e(ui)} + j\omega_m \Psi_{2s}^{e(ui)}, \quad (13)$$

where: the superscript “ $e(ui)$ ” denotes rotor flux space vector estimated by the voltage-current model, and the superscript “ e ” next to the stator current symbol indicates that this quantity is also estimated within the model.

Under steady state conditions, while replacing the complex frequency by the stator frequency $p = j\omega_1$, the rotor flux estimation FRF corresponding to the voltage-current model (12)–(13) can be expressed as a function of slip frequency like in (14) [21]. The $\text{FRF}^{(ui)}$ magnitude and phase characteristics are also presented in Fig. 2 and Fig. 3. According to Fig. 2, the rotor flux voltage-current model is characterized by limited sensitivity to rotor resistance deviations in a wider range of slip frequency in comparison to the current model. This fact can be explained by considering the $\text{FRF}^{(ui)}$ at high speeds $\omega_1 \gg \omega_2$. In this case the $\text{FRF}^{(ui)}$ takes the form presented in (15).

$$\text{FRF}^{(ui)} = \frac{\hat{\Psi}_{2s}^{e(ui)}}{\Psi_{2s}^{e(ui)}} = \frac{\left[\frac{R_1}{L_\mu} - \left(\frac{\sigma}{1-\sigma} \right) \frac{L_\mu}{R_2} \omega_1 \omega_2 \right] + j \left(\frac{R_1 L_2}{R_2 L_\mu} \omega_2 + \frac{L_1}{L_\mu} \omega_1 \right)}{\left[\frac{R_1}{L_\mu} - \left(\frac{\hat{\sigma}}{1-\hat{\sigma}} \right) \frac{L_\mu}{\hat{R}_2} \omega_1 \omega_2 \right] + j \left(\frac{R_1 \hat{L}_2}{\hat{R}_2 L_\mu} \omega_2 + \frac{L_1}{L_\mu} \omega_1 \right)} \Bigg|_{p=j\omega_1}, \quad (14)$$

$$\text{FRF}^{(ui)} \approx \left(1 + j\sigma \frac{L_2}{R_2} \omega_2 \right) \left(1 + j\hat{\sigma} \frac{\hat{L}_2}{\hat{R}_2} \omega_2 \right)^{-1} \Bigg|_{p=j\omega_1}. \quad (15)$$

The presence of the inductive leakage factor moved the slip frequency corresponding to the maximum sensitivity of the rotor flux voltage-current model to higher slip frequency values when compared to the current model (Fig. 2). In contrast, the rotor flux voltage-current model is more sensitive to rotor leakage inductance deviations than the current model (Fig. 3). However, this sensitivity occurs at higher slip frequency values which exceed the typical operating range of slip frequency for IM field-oriented control.

This fact makes the rotor flux voltage-current model a prospective candidate to the role of the adjustable model of the MRAS-based speed estimator which is intended for speed-sensorless IM drive applications. When assuming the conformity of the estimated stator current (12) with the actual one, the state error equation of the modified MRAS-based speed estimator can be expressed in analogous form as in [6]. Thus, the adaptation mechanism derived in [6] remains adequate to the modified MRAS-based speed estimator. In this case, the individual functions of the adopted adaptation mechanism take the following forms:

$$\Phi'_1(\varepsilon'_\alpha, \varepsilon'_\beta) = K_2 (\varepsilon'_\beta \Psi_{2\alpha}^{e(ui)} - \varepsilon'_\alpha \Psi_{2\beta}^{e(ui)}), \quad (16)$$

$$\Phi'_2(\varepsilon'_\alpha, \varepsilon'_\beta) = K_1 (\varepsilon'_\beta \Psi_{2\alpha}^{e(ui)} - \varepsilon'_\alpha \Psi_{2\beta}^{e(ui)}), \quad (17)$$

$$\varepsilon'_\alpha = \Psi_{2\alpha}^{e(u)} - \Psi_{2\alpha}^{e(ui)}, \quad (18)$$

$$\varepsilon'_\beta = \Psi_{2\beta}^{e(u)} - \Psi_{2\beta}^{e(ui)}. \quad (19)$$

The prime symbol is added to the adaptation mechanism functions and error equations (16)–(19) in order to distinguish them from the corresponding functions and error equations (5)–(8) developed for the classical MRAS-based speed estimator. The schematic diagram of

the investigated modification of the MRAS-based speed estimator is presented in Fig. 4. This configuration will be marked as the MRAS^(u-*ui*) throughout this paper.

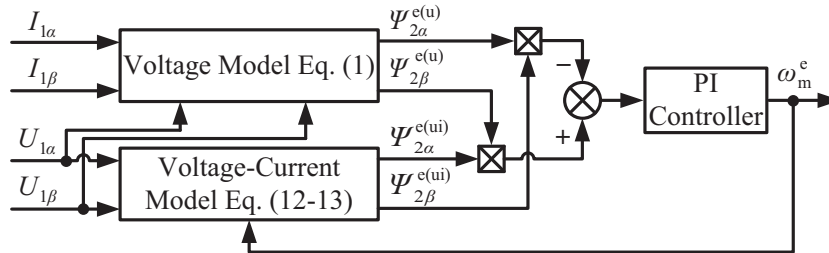


Fig. 4. The schematic diagram of the modified MRAS-based speed estimator

3. Laboratory setup and research methodology

The experimental investigations were realized in an open-loop drive system, at a fixed setpoint of stator voltages and step commands of load torque. The tested IMs were powered by the AC source AMETEK Model: 3001iX providing programmable sinusoidal output voltages. The load torque step commands were performed with the use of the programmable electronic load ZSAC4244 – H&H GmbH. Such a solution enabled shaping the desired dynamics of IM slip frequency changes in the assumed range. The armature current of a separately excited DC machine of type PCMb 54b was controlled so as to force changes of the IM stator currents in the range: no-load current up to 1.30 of rated current. The slip frequency range considered in the verification of the MRAS-based speed estimators corresponded also to the slip frequency range imposed during the load curve test which was performed to identify electromagnetic parameters of the tested IMs [22]. The schematic diagram of the laboratory test bench is presented in Fig. 5.

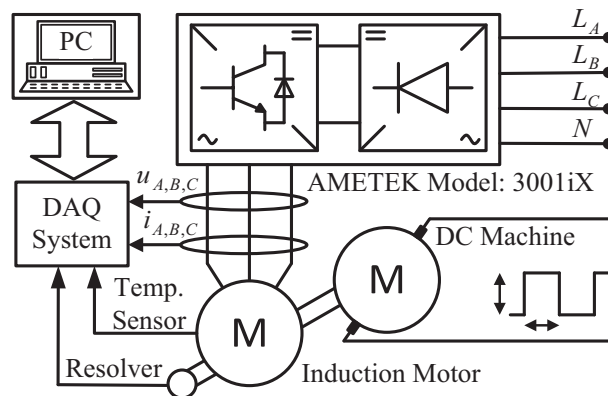


Fig. 5. The schematic diagram of the laboratory test bench

The investigations were conducted on the four-pole IM of type Sg 132S-4 with a squirrel-cage rotor and a solid rotor. The solid rotor was designed and manufactured for the purpose of the

conducted study since such a rotor is characterized by the intense skin effect. This approach enabled to verify the robustness of the analyzed MRAS-based speed estimators to rotor electromagnetic parameter variability resulting from the rotor deep-bar effect without employing a large squirrel-cage IM at this stage of the study. The rated values of the tested IMs corresponding to their adopted operating points are set together in Table A.1 included in the Appendix.

During the laboratory tests, the measurement of stator winding voltages, currents, and temperature, as well as IM speed, was performed. Data acquisition (DAQ) was done by means of a high-resolution, multifunction I/O device NI USB-6255 with the sampling frequency of 10 kHz. The DAQ system was equipped with the MAX7426 5th-order, lowpass, elliptic, switched-capacitor filters. The configuration of the DAQ device and the acquisition of measurement data were carried out in the National Instruments LabView environment.

Before starting the measurement tests, the investigated IMs operated at the given load torque for a period of time enabling to stabilize the stator winding temperature at the assumed level. It was done to reduce the impact of stator and rotor winding resistance variability, resulting from winding temperature changes, on the verification of IM speed estimation accuracy.

The mathematical models of the tested estimator configurations were implemented in the Matlab environment and solved with the fixed integration step corresponding to the DAQ sampling frequency. The electromagnetic parameters of the T-type Equivalent Circuit (T-EC), identified in accordance with the selected procedures described in the standards [23] (Set 1 and Set 3) and [24] (Set 2 and Set 4), are given in Table 1 and Table 2. These parameters were determined in vicinity of the adopted operating points of the investigated IMs (Table A.1). The stator phase resistance, determined through the DC line-to-line resistance measurement [23], after correction to the reference winding temperature of 25°C equalled $R_1 = 2.9597 \Omega$.

Table 1. The T-EC electromagnetic parameters of the tested squirrel-cage IM, rotor resistances are corrected to the reference winding temperature $T_{ref} = 25^\circ\text{C}$ [22]

| Electromagnetic parameters | $L_{1\sigma}$ (H) | L_μ (H) | R_2 (Ω) | $L_{2\sigma}$ (H) |
|----------------------------|-------------------|-------------|--------------------|-------------------|
| Set 1 | 0.0153 | 0.4999 | 1.5687 | 0.0230 |
| Set 2 | 0.0147 | 0.5041 | 1.6973 | 0.0219 |

Table 2. The T-EC electromagnetic parameters of the tested solid rotor IM, rotor resistances correspond to the average temperature of stator winding $T_{ref} = 55^\circ\text{C}$ registered under the load curve test [22]

| Electromagnetic parameters | $L_{1\sigma}$ (H) | L_μ (H) | R_2 (Ω) | $L_{2\sigma}$ (H) |
|----------------------------|-------------------|-------------|--------------------|-------------------|
| Set 3 | 0.0423 | 0.4613 | 11.5581 | 0.0741 |
| Set 4 | 0.0268 | 0.5169 | 19.7569 | 0.0400 |

The IM speed estimation accuracy was verified based on the relative errors between the measured and estimated speed (20). For better assessment of the operation accuracy of the analyzed speed estimation schemes, the maximal and mean relative speed estimation errors were

additionally determined according to Equations (21) and (22), respectively.

$$\Delta\omega_m^e = \frac{\omega_m - \omega_m^e}{\omega_m} 100\%, \quad (20)$$

$$\max |\Delta\omega_m^e| = \max \left| \frac{\omega_m - \omega_m^e}{\omega_m} 100\% \right|, \quad (21)$$

$$M |\Delta\omega_m^e| = \frac{1}{n} \sum_{i=1}^n \left| \frac{\omega_{m,i} - \omega_{m,i}^e}{\omega_{m,i}} 100\% \right|, \quad (22)$$

where: $\omega_{m,i}$, $\omega_{m,i}^e$ are the i -th samples of the measured and estimated speed, respectively, and n is the number of samples.

4. Results of experimental tests

In the first instance, the evaluation of IM speed estimation accuracy obtained by the MRAS^(u-i) was performed. Fig. 6(a) shows the registered and estimated speed of the squirrel-cage IM whereas Fig. 6(b) presents the speed estimation relative errors. The measured and estimated speed of the solid rotor IM and also the speed estimation relative errors are included in Fig. 7(a) and Fig. 7(b), respectively. Additionally, the maximal and mean relative errors introduced by the considered configurations of the MRAS-based speed estimator are set together in Table 3 for both tested IMs. It should be noted that the IM speed presented in figures included in this section is expressed in the per-unit system. The synchronous speed of the tested IMs was used as the base value.

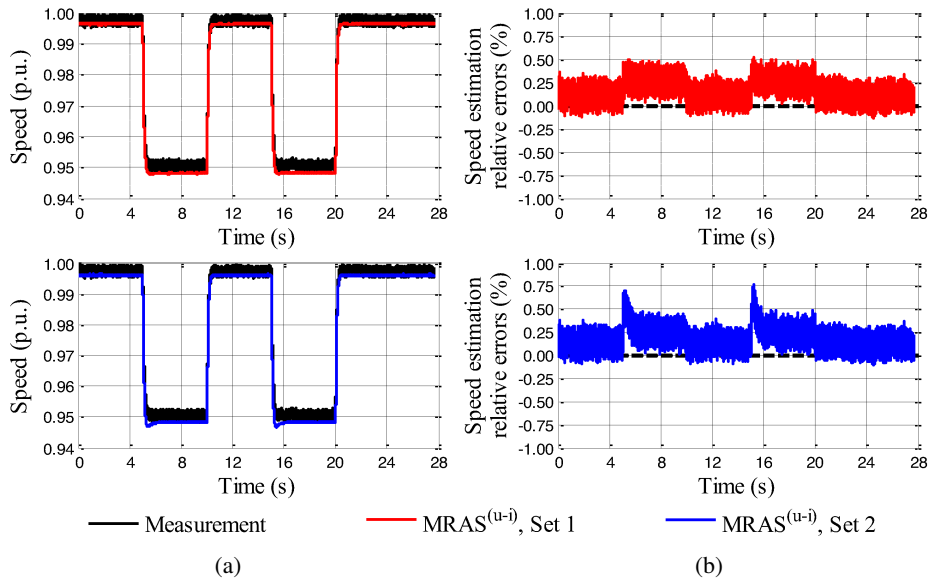


Fig. 6. The squirrel-cage IM speed estimation conducted by the MRAS^(u-i): (a) the registered and estimated speed; (b) the speed estimation relative errors

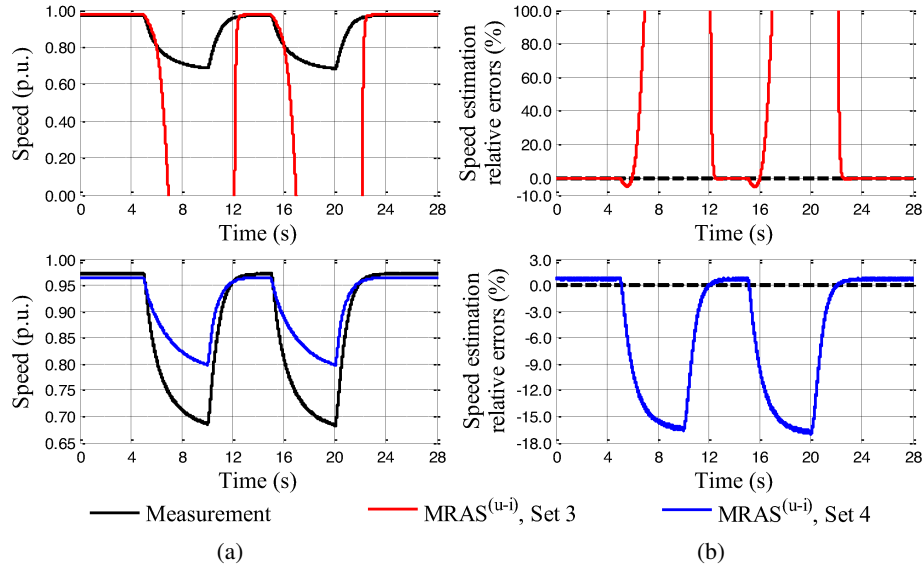


Fig. 7. The solid rotor IM speed estimation conducted by the MRAS^(u-i): (a) the registered and estimated speed; (b) the speed estimation relative errors

The MRAS^(u-i) enabled the speed estimation of the squirrel-cage IM with relative errors not exceeding $\pm 1\%$ (Table 3) in the considered range of slip frequency, no matter which sets of the electromagnetic parameters were used in the estimator mathematical model (Table 1).

Table 3. The maximal and mean relative errors of the measured speed estimation

| Tested IM | Squirrel-cage IM | | | | Solid rotor IM | | | |
|------------------------------|-----------------------|--------|------------------------|--------|-----------------------|---------|------------------------|--------|
| | MRAS ^(u-i) | | MRAS ^(u-ii) | | MRAS ^(u-i) | | MRAS ^(u-ii) | |
| Estimation schemes | Set 1 | Set 2 | Set 1 | Set 2 | Set 3 | Set 4 | Set 3 | Set 4 |
| max $ \Delta\omega_m^e $ (%) | 0.5173 | 0.7709 | 0.3654 | 0.5954 | > 100.0 | 17.0387 | 4.4336 | 1.4919 |
| M $ \Delta\omega_m^e $ (%) | 0.1735 | 0.1935 | 0.0899 | 0.2216 | > 100.0 | 5.8326 | 1.2105 | 1.0228 |

In relation to the solid rotor IM, the employment of the MRAS^(u-i) with Set 3 of the electromagnetic parameters (Table 2) did not provide the correct speed estimation when the tested motor operated under load (Fig. 7(a)). This fact confirms the theoretical considerations included in [7, 8] which pointed out the tendency of the MRAS^(u-i) to lose stability in the case of erroneous representation of the IM electromagnetic parameters by equivalent parameters applied in the estimator mathematical model. The MRAS^(u-i) with Set 4 of the electromagnetic parameters (Table 2) operated stably throughout the considered range of slip frequency, however the estimated speed of the solid rotor IM was fraught with errors reaching 17% (Table 3) when the motor was loaded up to 1.30 of the stator rated current (Fig. 7).

During the next step of the study, the speed estimation conducted by means of the $MRAS^{(u-ii)}$ was verified. Figs. 8 and 9 present the measured and estimated speed as well as the speed estimation relative errors of the investigated IM with the squirrel-cage and solid rotors, respectively.

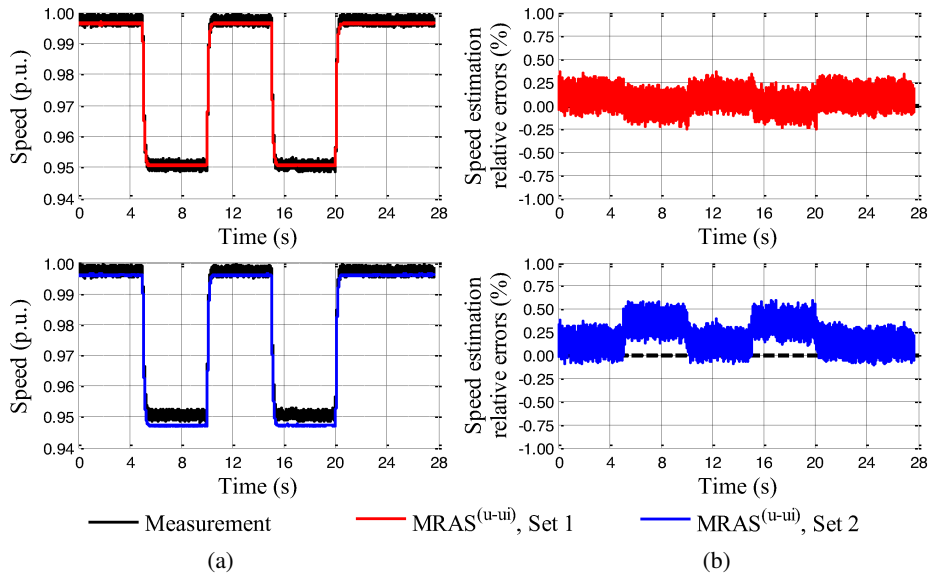


Fig. 8. The squirrel-cage IM speed estimation conducted by the $MRAS^{(u-ii)}$: (a) the registered and estimated speed; (b) the speed estimation relative errors

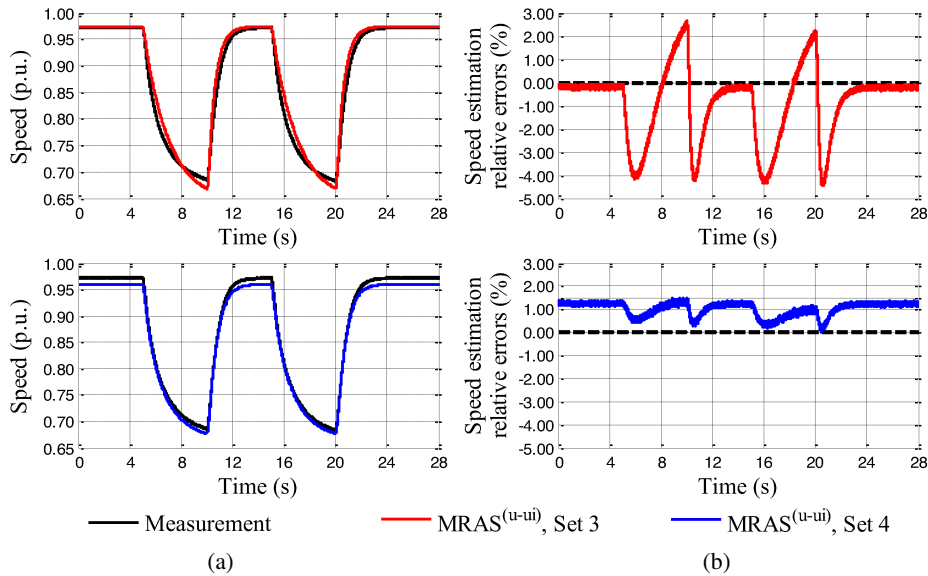


Fig. 9. The solid rotor IM speed estimation conducted by the $MRAS^{(u-ii)}$: (a) the registered and estimated speed; (b) the speed estimation relative errors

The MRAS^(u-*ui*) also enabled the speed estimation of the squirrel-cage IM with relative errors not exceeding $\pm 1\%$ (Table 3) in the considered range of slip frequency. However, it should be pointed out that this configuration of the MRAS-based speed estimator allowed further limitation of speed estimation relative errors (Fig. 6, Fig. 8, Table 3), in case when Set 1 of the electromagnetic parameters (Table 1) were applied in the estimator mathematical model.

It is worth to note that the use of the rotor flux voltage-current model as the adjustable model in the MRAS-based speed estimator allowed the speed estimation of the solid rotor IM with considerably lower errors (less than $\pm 5\%$) than the MRAS^(u-*i*) (Fig. 7, Fig. 9, Table 3). Further, the employment of Set 4 of the electromagnetic parameters (Table 2) in the MRAS^(u-*ui*) enabled to reduce the speed estimation relative errors to $\pm 1.5\%$ (Table 3) in the considered range of slip frequency.

5. Conclusions

The results of the laboratory tests prove that the use of the rotor flux voltage-current model in lieu of the current model in the MRAS-based speed estimator allowed to improve the speed estimation accuracy and reliability of the analyzed IMs in the considered range of slip frequency. Thus, the proposed modification of the MRAS-based speed estimator reduced its sensitivity to the variability of rotor electromagnetic parameters resulting from the rotor-deep bar effect. This is particularly evident for the tested IM characterized by the intense rotor skin effect. It is also worth noting that the improvement of the speed estimation performance is achieved with maintaining the similar algorithm complexity of the modified MRAS-based speed estimator when compare to the classical one. For these reasons, the modified MRAS-based speed estimator can be considered for IM drive applications, especially these employing IMs characterized by the intense rotor deep-bar effect like large squirrel-cage IMs.

Appendix

Table A1. Operating data of the tested induction motor of type Sg 132S-4 with a cage rotor and a solid rotor corresponding to the adopted machine operating points

| Parameters | Unit | Squirrel-cage IM | Solid rotor IM |
|------------------|-------|------------------|----------------|
| Output power | (kW) | 2.358 | 1.992 |
| Stator voltage | (V) | 400 (wye) | 400 (delta) |
| Stator frequency | (Hz) | 50 | 85 |
| Stator current | (A) | 4.536 | 7.785 |
| Rotational speed | (rpm) | 1450 | 2030 |

Acknowledgements

This work was supported by the Polish Ministry of Science and Higher Education under research projects: BS/MN-401-312/15 and 03.0.00.00/2.01.01.0001MNSPE.19.001.

References

- [1] Xu D., Wang B., Zhang G., Wang G., Yu Y., *A review of sensorless control methods for AC motor drives*, CES Transactions on Electrical Machines and Systems, vol. 2, no. 1, pp. 104–115 (2018).
- [2] Aiello M., Cataliotti A., Nuccio S., *An induction motor speed measurement method based on current harmonic analysis with the chirp-Z transform*, IEEE Transactions on Instrumentation and Measurement, vol. 54, no. 5, pp. 1811–1819 (2005).
- [3] Zhao L., Huang J., Chen J., Ye M., *A Parallel Speed and Rotor Time Constant Identification Scheme for Indirect Field Oriented Induction Motor Drives*, IEEE Transactions on Power Electronics, vol. 31, no. 9, pp. 6494–6503 (2016).
- [4] Joy M.T., Böcker J., *Sensorless Control of Induction Motor Drives Using Additional Windings on the Stator*, IEEE 9th International Symposium on Sensorless Control for Electrical Drives, Helsinki, Finland, pp. 162–167 (2018).
- [5] Song X., Wang Z., Li S., Hu J., *Sensorless Speed Estimation of an Inverter-Fed Induction Motor Using the Supply-Side Current*, IEEE Transactions on Energy Conversion, vol. 34, no. 3, pp. 1432–1441 (2019).
- [6] Schauder C., *Adaptive speed identification for vector control of induction motors without rotational transducers*, IEEE Transactions on Industry Applications, vol. 28, no. 5, pp. 1054–1061 (1992).
- [7] Niestrój R., Białoń T., Pasko M., *Stability analysis of the MRAS-type estimator taking into consideration parameter changes of the model of the induction motor* (in Polish), Zeszyty Naukowe Politechniki Śląskiej, Elektryka, vol. 216, no. 4, pp. 39–53 (2010).
- [8] Orłowska-Kowalska T., Dybkowski M., *Stator-current-based MRAS estimator for a wide range speed-sensorless induction-motor drive*, IEEE Transactions on Industrial Electronics, vol. 57, no. 4, pp. 1296–1308 (2010).
- [9] Gadoue S.M., Giaouris D., Finch J.W., *Stator current model reference adaptive systems speed estimator for regenerating-mode low-speed operation of sensorless induction motor drives*, IET Electric Power Applications, vol. 7, no. 7, pp. 597–606 (2013).
- [10] Zbede Y.B., Gadoue S.M., Atkinson D.J., *Model Predictive MRAS Estimator for Sensorless Induction Motor Drives*, IEEE Transactions on Industrial Electronics, vol. 63, no. 6, pp. 3511–3521 (2016).
- [11] Kumar R., Das S., Chattopadhyay A.K., *Comparative assessment of two different model reference adaptive system schemes for speed-sensorless control of induction motor drives*, IET Electric Power Applications, vol. 10, no. 2, pp. 141–154 (2016).
- [12] Rolek J., Utrata G., Kaplon A., *Improving robustness of the MRAS-based speed estimator to variability of induction motor electromagnetic parameters resulting from the rotor deep bar effect*, 14th Selected Issues of Electrical Engineering and Electronics (WZEE 2018), Szczecin, Poland (2018).
- [13] Das S., Kumar R., Pal A., *MRAS-based speed estimation of induction motor drive utilizing machines' d- and q-circuit impedances*, IEEE Transactions on Industrial Electronics, vol. 66, no. 6, pp. 4286–4295 (2019).
- [14] Reddy C.U., Prabhakar K.K., Singh A.K., Kumar P., *Speed Estimation Technique Using Modified Stator Current Error Based MRAS for Direct Torque Controlled Induction Motor Drives*, IEEE Journal of Emerging and Selected Topics in Power Electronics (2019), DOI: 10.1109/JESTPE.2019.2901523.
- [15] Marčetić D.P., Vukosavić S.N., *Speed-sensorless AC drives with the rotor time constant parameter update*, IEEE Transactions on Industrial Electronics, vol. 54, no. 5, pp. 2618–2625 (2007).
- [16] Harnefors L., Hinkkanen M., *Complete stability of reduced-order and full-order observers for sensorless IM drives*, IEEE Transactions on Industrial Electronics, vol. 55, no. 3, pp. 1319–1329 (2008).

- [17] Zaky M.S., Metwaly M.K., Azazi H.Z., Deraz S.A., *A New Adaptive SMO for Speed Estimation of Sensorless Induction Motor Drives at Zero and Very Low Frequencies*, IEEE Transactions on Industrial Electronics, vol. 65, no. 9, pp. 6901–6911 (2018).
- [18] Chen J., Huang J., *Stable Simultaneous Stator and Rotor Resistances Identification for Speed Sensorless IM Drives: Review and New Results*, IEEE Transactions on Power Electronics, vol. 33, no. 10, pp. 8695–8709 (2018).
- [19] Zerdali E., Barut M., *The Comparisons of Optimized Extended Kalman Filters for Speed-Sensorless Control of Induction Motors*, IEEE Transactions on Industrial Electronics, vol. 64, no. 6, pp. 4340–4351 (2017).
- [20] Yin Z., Li G., Zhang Y., Liu J., *Symmetric-Strong-Tracking-Extended-Kalman-Filter-Based Sensorless Control of Induction Motor Drives for Modeling Error Reduction*, IEEE Transactions on Industrial Informatics, vol. 15, no. 2, pp. 650–662 (2019).
- [21] Jansen P.L., Lorenz R.D., *A physically insightful approach to the design and accuracy assessment of flux observers for field oriented induction machine drives*, IEEE Transactions on Industry Applications, vol. 30, no. 1, pp. 101–110 (1994).
- [22] Rolek J., Utrata G., *An identification procedure of electromagnetic parameters for an induction motor equivalent circuit including rotor deep bar effect*, Archives of Electrical Engineering, vol. 67, no. 2, pp. 279–291 (2018).
- [23] Standard PN-EN 60034-28:2012, *Rotating Electrical Machines – Part 28: Test methods for determining quantities of equivalent circuit diagrams for three-phase low-voltage cage induction motors* (2012).
- [24] IEEE Standard 112TM-2004, *IEEE Standard Test Procedure for Polyphase Induction Motors and Generators* (revision of IEEE Std 112-1996), IEEE Power Engineering Society, New York, USA (2004).